Scenario-based inundation analysis of metro systems: a case study in Shanghai

Hai-Min Lyu[1], Shui-Long Shen[1,2], Jun Yang[3], Zhen-Yu Yin[4]

[1]State Key Laboratory of Ocean Engineering, School of Naval Architecture, Ocean, and Civil Engineering, Shanghai Jiao Tong University, Shanghai 200240, China

[2]Department of Civil and Environmental Engineering, College of Engineering, Shantou Univ., Shantou, Guangdong 515063, China

[3]Department of Civil Engineering, The University of Hong Kong, Pokfulam, Hong Kong, China

[4]Department of Civil and Environmental Engineering, The Hong Kong Polytechnic University, Hung Hom, Kowloon, Hong Kong, China

Correspondence to: Shui-Long Shen (slshen@sjtu.edu.cn)

Abstract. Catastrophic urban floods result in severe inundation of underground facilities in recent years. This paper presents an integrated approach in which an algorithm is proposed to integrate the storm water management model (SWMM) into the geographical information system (GIS) to evaluate the inundation risk. The proposed algorithm simulates the flood inundation of overland flow and metro station for each schemed scenario. It involves *i*) determination of the grid location and spreading coefficient and *ii*) iterative calculation of the spreading process. In addition, an equation is proposed to qualitatively calculate the inundation around a metro station to predict the potential inundation risks of metro systems. This equation considered the drainage capacity and characteristics of each metro station. The proposed method is applied to simulate the inundation risks of the metro system in the urban centre of Shanghai under 50-year, 100-year, and 500-year scenarios. Both the inundation extent and depth are derived. The proposed method is validated by verifying from the records of historical floods. The results demonstrate that in case of the 500-year-rainfall scenario, for an inundation depth of over 300 mm, the inundated area is up to 5.16 km^2, which is 4.3% of the studied area and that there are four metro stations inundated to a depth of over 300 mm.

Keywords: urban inundation, scenario analysis, metro system, algorithm for overland flow, SWMM, GIS

1. Introduction

With rapid urbanization, numerous urban constructions (e.g., underground metro system, malls, infrastructural systems, and parks) have been built (Peng and Peng, 2018). The disturbance caused by underground constructions (Shen et al. 2014, 2017; Tan et al. 2017) makes the geological environment susceptible to natural hazards, e.g., floods, tornados, and typhoons (Chang et al. 2010; Lyu et al. 2016, 2017). In recent years, climate change has resulted in various rainstorm events in China (Zhou et al. 2012; Yin et al. 2018; Xu et al. 2018). Many metropolitan areas have frequently suffered from inundation due to urban flooding. Urban flooding is one of the most severe hazards which causes catastrophic submerging of the ground surface and severe inundation of underground facilities. Numerous metro lines were inundated during the flood season (May to September) in 2016 in China, such as the metro lines in Guangzhou and Wuhan. The Shanghai Station of metro line No.1 was inundated on October 3, 2016 (Lyu et al. 2018a, b). Prevention of metro systems from inundation is an urgent challenge which needs to be solved during urban planning (Huong and Pathirana 2013). Thus, the prediction of the inundation of a metro system is of critical importance.

There are generally four methods to predicting the inundation risk: (1) statistical analysis based on historical disaster records (Nott 2006), (2) geographical information system and remote sensing (GIS-RS) techniques (Sampson et al. 2012; Meesuk et al. 2015), (3) multi-criteria index analysis (Jiang et al. 2009; Kazakis 2015), and (4) scenario inundation analysis (Willems 2013; Naulin et al. 2013). Although the assessment results based on historical disaster records can predict the risk of an area, the method needs large numbers of data (Nott 2006). GIS-RS can provide the technological support for inundation risk evaluation (Sampson et al. 2012; Meesuk et al. 2015); however, GIS-RS technologies require high investments and high-resolution data sources. Multi-criteria index analysis has a few limitations in the determination of subjective indices (Jiang et al. 2009; Kazakis 2015). Scenario-based inundation analysis

predicts inundation risk under different scenarios (Willems 2013; Naulin et al. 2013; Wu et al., 2018), which requires the topography, land-use, and urban drainage system data. Owing to the complex interaction between the drainage system and overland surface in urban regions, scenario-based models can only simulate inundation over a small range, e.g., less than 3 km^2 (Wu et al. 2017), which limits their application. Thus, the application of scenario-based model needs to be extended to the problem of overland flow over a large scale, e.g. whole region with area over several hundred square kilometers.

Numerical simulation is a useful tool to analyse urban flooding. Xia et al. (2011) developed a numerical model which integrated an algorithm into a two-dimensional (2D) hydrodynamic model to assess flood risk. Szydlowski et al. (2013) proposed a numerical flood modelling in which a mathematical model was incorporated into a 2D hydrological model to estimate inundation risks. Chen et al. (2015) used numerical simulation to predict the inundation risk in a flood-prone coastal zone. Morales-Hernandez et al. (2016) presented a one-dimensional model coupled with a two-dimensional model (1D-2D model) for application in the fast computation of large-river flooding. However, these numerical models have the following shortcomings: i) it is difficult to consider the characteristics of the landform, and ii) numerical simulation is typically used to estimate the inundation risk in a small area, whereas flooding hazards often occur on a regional scale. Thus, most of these models can only simulate inundation in a small range (Horritt and Bates 2002; Han et al. 2014). Moreover, the existing numerical studies cannot identify the boundary, resulting in a large error because the boundary is in extreme vicinity of the area centre. Therefore, a new tool, e.g., GIS, is required to consider the characteristics of a landform, and an integrated method should be proposed to simulate regional-scale flooding and satisfy the boundary conditions.

The storm water management model (SWMM) is a dynamic hydrological model, which is widely used for simulating the rainfall–runoff process in an urban catchment (Hsu et al. 2000; Shen and Zhang 2015; Bisht et al., 2016; Ai-Mashaqbeh and Shorman, 2019; Zhao et al., 2019). However, till date, the SWMM

has achieved this for only a small region of several square kilometres. For example, Zhu et al. (2016) used the SWMM and a multi-index system to evaluate the inundation risks in southwest Guangzhou, China, in an area of 0.43 km^2. Feng et al. (2016) selected the SWMM as the modelling platform to simulate the inundation risks in a campus of the Salt Lake City, Utah, U.S, in an area of 0.11 km^2. Wu et al. (2017) applied the SWMM in combination with Lisflood-FP to simulate the urban inundation in Dongguan city, China, within an area of 2 km^2. It is challenging to predict the potential inundation risks on a regional scale using the SWMM because it is difficult to determine the spreading process and flow direction of the runoff on a large scale. Thus, a new method needs to be proposed which can the predict inundation risk on a regional scale using the SWMM.

Till date, there are a few published research studies, which focused on the inundation risk of metro systems. Yanai (2000) and Hashimoto (2013) analysed the flood event in Fukuoka city in 1999, which led to the serious inundation of the metro station. Based on previous research, Aoki (2016) put forward anti-inundation measures to prevent inundation for the stations of the Tokyo metro. Herath and Dutta (2004) attempted to create a model of urban flooding including underground space. Suarez et al. (2005) undertook a risk assessment of flooding for the Boston metro area. Ishigaki et al. (2009) presented a method for the safety assessment of a Japanese metro. Therefore, the research on the investigation of the inundation risk of metro systems is insufficient.

The objectives of this study are to: *i*) propose a method for predicting the potential inundation risk on a regional scale by using an new algorithm to integrate the SWMM into the GIS to simulate the overland flow, *ii*) propose a method for evaluating the potential inundation risk of a metro system, and iii) apply the proposed method to simulate the scenarios of urban inundation and inundation depth for the Shanghai metro system in case of 50-year, 100-year, and 500-year-rainstorm events. The proposed method assumes that the runoff on the surface flows from one subcatchment to another, within the range serviced by the

drainage station.

2. Materials

2.1 Study area

Shanghai locates between latitudes 31°20′ and 31°00′N at longitude 121°20′ to 121°31′E, with a region of more than 6340 km^2. Fig. 1 shows the administrative region of Shanghai. As illustrated in Fig. 1, the Shanghai metropolis is surrounded by the Yangtze River in the northeast, Hangzhou bay in the southeast, Zhejiang province in the west, and Jiangsu province in the northwest (Shen and Xu 2011). The average elevation is ranged from 2 m to 5 m above the sea level in Shanghai (Xu et al. 2016). The urban centre with area of 120 km^2 includes the districts of Jingan, Huangpu, Luwan, Xunhui, Changning, Putuo, Zhabei, Hongkou, and Yangpu. Metro line No. 1 was constructed in Shanghai between 1990 and 1995. The first metro line from Xujiahui station to Jinjiang Park station was opened for operation on 28 May, 1993. At present, there are 14 metro lines under operation (data from Planning of Shanghai Metro Line, 2016) and another eight metro lines are currently under construction. As shown in Fig. 1, the urban centre with a dense distribution of metro lines. Moreover, the urban centre is near the Huangpu River, which passes through Shanghai city. There are also several metro lines passing through the Huangpu River. The rising tide in the Huangpu River increases the risk of floods, particularly during the flood season (from June to July). As significant underground infrastructures, metro lines play important roles at the traffic junctions in mega-cities. During flooding disasters, metro lines will be crippled, resulting in severe impacts such as traffic paralysis.

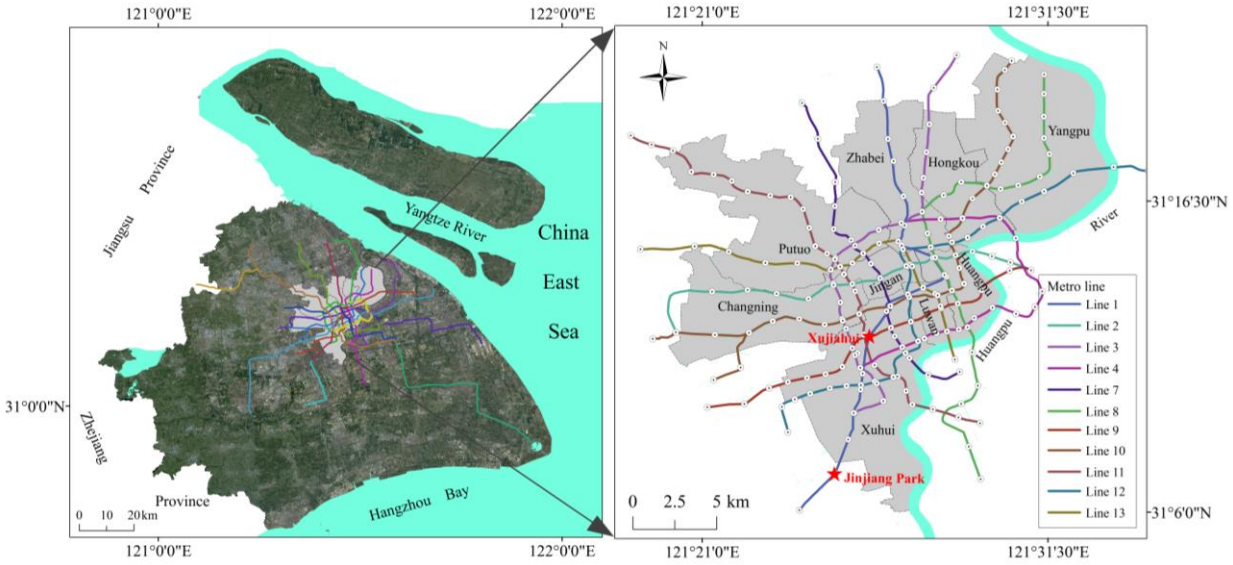

Figure 1: Distribution of metro line in the study area of Shanghai

2.2 Precipitation data and processing

Precipitation is the external driving force inducing flooding disasters. The Chicago design storm (Yin et al. 2016a, b) is widely applied to produce precipitation, which is used to calibrate the peak intensity and precipitation before and after the peak, within different return periods of the rainfall. The equations for the Chicago design storm can be expressed as follows:

$$i_a = \frac{a \times [\frac{(1-c) \times t_a}{1-r} + b]}{(\frac{t_a}{1-r} + b)^{c+1}} \quad (1)$$

$$i_b = \frac{a \times [\frac{(1-c) \times t_b}{r} + b]}{(\frac{t_b}{r} + b)^{c+1}} \quad (2)$$

where, i_a and i_b are the precipitation intensities after and before the peak value (mm/min); t_a and t_b are the times after and before the peak value (min); a, b and c are specific values related to the local municipal rainstorm models of the intensity-duration-frequency (IDF) type.

Based on documentary investigation, the IDF of the Shanghai municipal rainstorm can be expressed as follows (Jiang et al., 2015):

$$i = \frac{9.581(1+0.846\lg T)}{(t+70)^{0.656}} \tag{3}$$

where i is the precipitation intensity (mm/min), T is the return period of precipitation (year), and t is the duration of the precipitation (min).

To consider the temporal variations, parameter r (e.g., the ratio of the time for the peak to the total event duration) is fixed as 0.45 (Yin et al., 2016a). The rainfall intensity for a duration of 2 h and return periods of the scenarios for 50 years, 100 years, and 500 years are designed to model the probable inundation. The drainage capacity of the metro line is designed to be 90 mm/h (the period of a 50-year-flooding event).

2.3 Topographical data and drainage station

The digital elevation model (DEM) of the study region was available with a 30-m-resolution, which was obtained from the geospatial data cloud. To replicate the reality of the study area, the DEM was further modified in the region with buildings based on field surveys and documents (Yin et al. 2016a). The heights of the buildings were rebuilt in the DEM to reproduce the blockage effects on the surface flows. The distribution of the drainage stations was obtained from the Shanghai Municipal Sewerage Management Branch (Quan et al. 2011).

3. Methodology

The proposed approach to predicting the inundation risk of metro system includes three phases. The first, a simulated rainfall runoff volume is obtained using SWMM model. The second, the calibrated runoff volume is distributed using the proposed spreading procedure algorithm, which integrates SWMM into GIS to determine the surface inundation depth. The third, the inundation depth around a metro station was

obtained using the proposed equation and GIS tools (e.g., grid calculation, and extract multi values to points, etc).

3.1 SWMM calibration

The SWMM model is widely used to simulate the runoff quantity produced in each subcatchment in a simulated period. The results obtained by SWMM model were closer to measured value, and which can indicate the runoff reached a peak in the shortest time (Lee et al. 2010). The previous researches show that the SWMM is one of the best hydrologic models (Tan et al., 2008; Cherqui et al., et al., 2015). In this study, the SWMM is used to calibrate the runoff volumes from each subcatchment. It is supposed that, under extreme rainfall scenarios, runoff concentrates at the outlet point of each catchment and ignore the function of the drainage network. In this case, the overland flow is more likely to move in multiple directions rather than through the predefined flow paths and outlets. Therefore, a coefficient in the spreading process algorithm was used to determine the flow paths on surface. The spreading coefficient is used for moving runoff between neighbor subcatchments. Moreover, the function of drainage network is reflected by the drainage capacity of each drainage station (see Fig. 2). The water quantity of each subcatchment calculated in SWMM is reduced by the capacity of the drainage station. The detailed information about the algorithm is introduced in section 3.2.

3.1.1 Subcatchment division and flow direction

A subcatchment is the basic calculation cell in the SWMM. There are two types of subcatchment divisions (Shen and Zhang 2015): i) based on the subcatchment partition and ii) based on the drainage system. In this study, a subcatchment was initially divided using the Thiessen polygon method based on the spatial distribution of the drainage stations (Shen and Zhang 2015; Zhu et al. 2016). The drainage capacity of each subcatchment was determined by the service range of the drainage stations. The boundary was a fixed boundary, i.e., the water level at the boundary is not considered to spread because the attention point

is sufficiently far from the boundary. Fig. 2 shows the characteristics of subcatchment and grid in SWMM and GIS. The study area was classified into different subcatchment based on the drainage capacity of the pumping station service (Fig. 2a). Each subcatchment was classified into grid with 20 m×20 m (Fig. 2b), and each grid has its own information to reflect the different characteristic. To realistically mimic the effect of the natural hydrology features of a subcatchment, the topographical characteristics of the catchment was paid attention in the process of subcatchment division. The flow direction of each subcatchment was determined based on the DEM. Following this procedure, the average elevation and slope of each subcatchment was extracted by GIS tools. To reproduce the obstacles from the buildings in the flow of the surface runoff, the elevation included the height of the building and the building location in the model. Therefore, the average slope of a subcatchment will be reflective of the obstacle imposed by a building in the flow of the rainwater.

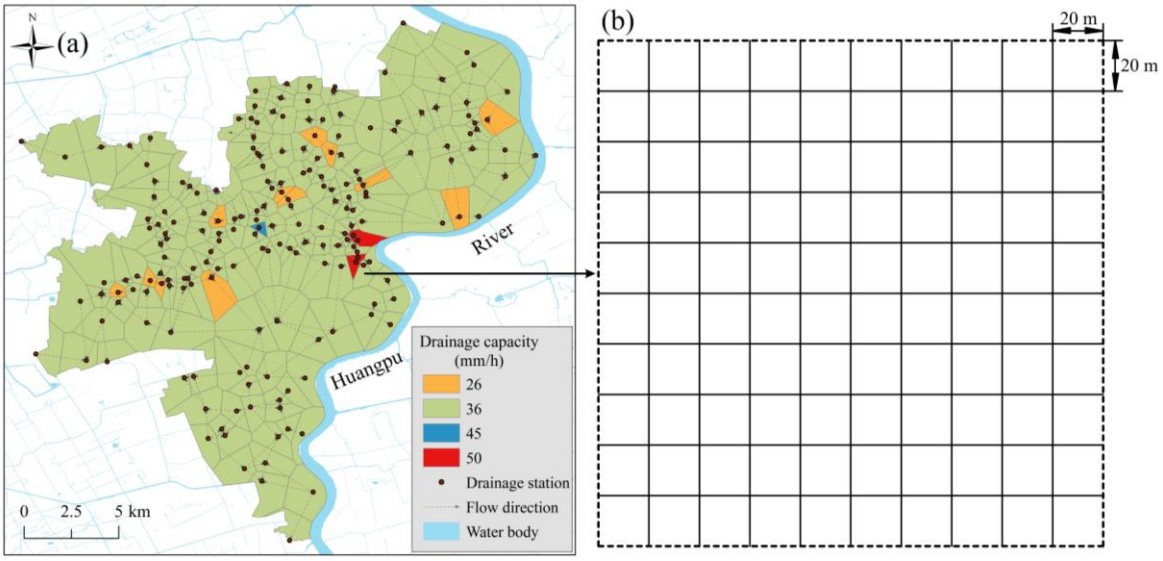

Figure 2: Calculated subcatchment and grid in SWMM and GIS: (a) drainage capacity and flow direction of each subcatchment; (b) calculated grid of each subcatchment

3.1.2 Model input and determination of parameters

Based on the aforementioned method of subcatchment division, each subcatchment was assigned with its own topographical characteristics. The model included 195 subcatchments and 204 junctions. Each subcatchment in the SWMM model included the parameters of width, area, and permeability. The width and area can be calculated by GIS tools. Table 1 tabulates the parameters of the subcatchments in the SWMM. The impervious parameter was determined based on the types of land use. The study area is located in urban centre, where the land use has no big changes. The existence of dense buildings in the study area makes more than 80% of the surface is impervious. Due to the existence of road pavement, subgrade and many municipal pipelines under the road, the water infiltration through road and subsurface under road is very small, which can be considered as impervious. Thus, soil infiltration and evapotranspiration have slight effects on surface runoff concentration during short-term flash flooding under rainstorm. The soil infiltration mainly depends on green land (combined by lawn, flower bed, and grove) and water body within the study area. In this aspect, the geotechnical information in Shanghai is as follows. The groundwater table is higher than 2 m below ground surface. The soil type at the depth 2 m is a mixed soil with of sand (5%), silt (55%), and clay (40%) according to Shanghai Geotechnical Investigation Code (DGJ08-37-2012). At the surface, sand content increased to 15%, so that soil has the hydraulic conductivity of 2×10^{-5} m/s, which is 72 mm/h; at the bottom of water body, the soil has more clay content (>50%) and less sand content (<5%) with the hydraulic conductivity of 2×10^{-7} m/s, which is 0.72 mm/h (Shen et al., 2015). According to the SWMM handbook, the maximum infiltration rate is determined as 72 mm/h to reflect the characteristics of green land, while the minimum value is 0.72 mm/h to reflect the characteristics of water body, since the soil under water body is saturated clay. In addition, the blocking effects of the buildings have significant influences on the surface runoff generation and concentration. Therefore, the heights of the existing buildings were extracted to modify the elevation of the calculated grids, which have crucial influence on the redistribution of rainwater during calculation.

Table 1 Parameters of the subcatchments in the SWMM

Parameter	Meaning	Value
Area (km^2)	Area of each subcatchment	10.38–0.16
Width (m)	Width of each subcatchment	5283.83–432.45
Impervious (%)	Percentage of the impervious area	65–80
Slope (°)	Average slope of each subcatchment	0.3–5.5
Destore-impervious (mm)	Depression storage depth in the impervious area	1.5
Destore-pervious (mm)	Depression storage depth in the previous area	5
N-impervious	Manning's coefficient in the impervious area	0.1
N-pervious	Manning's coefficient in the previous area	0.24
MaxRate (mm/h)	Maximum infiltration rate	72
MinRate (mm/h)	Minimum infiltration rate	0.72
Decay (h^{-1})	Decay constant	4
Dry (d)	Drying time	2

3.2 Data conversion between GIS and SWMM

Following the calibration of runoff volume of each subcatchment, the next step is to determine the spreading procedure of the calibrated runoff. The spreading procedure algorithm is used to integrate the data between GIS and SWMM. Fig. 3 shows the description of the spreading procedure of runoff. Fig. 3(a) illustrates the determination of grid location and spreading coefficient. Fig 3(b) is the iterative calculation of the spreading process. First, grids are created with 20 m×20 m meshes across the study area using GIS fishnet tools [see Fig. 3(a)]; second, the calculated average inundation depth is extracted from each grid [see Fig. 3(b)]. The study area includes 113810 grids. As shown in Fig. 3(b), the spreading procedure includes four steps. The detailed steps are described as follows:

Step 1: The grid location (*GL*) and spreading coefficient (*f*) are determined (see Fig. 3a). Assuming that each grid h_I is surrounded by h_{Ij} grids (j = 1, 2,…8), if $h_I + \Delta x = h_{Ij}$ or $h_I + \Delta y = h_{Ij}$, then the location of grids h_{Ij} are determined as GL = 1 and spreading coefficient f = 1. However, if $h_I + \Delta x = h_{Ij}$ and $h_I + \Delta y = h_{Ij}$, then the location of grids h_{Ij} is determined as GL = -1 and spreading coefficient f = 0.569.

Step 2: The spreading grid is ranked. In this process, the rank of a spreading grid is based on the value of the possible water quantity of target grid h_I from surrounding grids h_{Ij}, and it can be described by Eq. (4). It is assumed that the grid with the maximum quantity is the first spreading grid.

$$Q_{target} = \sum_{j=1}^{n} h_{Ij} \cdot a_j \cdot f \quad (n = 1, 2, \cdots, 8) \tag{4}$$

in which, Q_{target} is the runoff of the target j grid; h_{Ij} means there are j grids surrounding with the h_I grid; a_j is the area of j grid (in this study a_j=400 m^2); f is the spreading coefficient.

Step 3: Spreading and updating of the water level in each grid is started. It is assumed that the water level difference in each spreading step is Δh (Δh can be fixed as a specific or flexible value). The amount of water quantity in each spreading step can be described by Eq. (5). To ensure the convergence of the calculation process, the value of Δh can be fixed as some small value in the initial stage and then allowed to increase with time. In this algorithm, initial value Δh is fixed as 0.01.

$$Q_{spreading} = \sum_{j=1}^{n} (h_I - h_{Ij}) \cdot a_j \quad (n=1,2,\cdots,8) \tag{5}$$

in which, $Q_{spreading}$ is the runoff of surrounding grids.

Step 4: Cessation of the spreading is estimated. When the water level difference between target grid h_I and surrounding grid h_{Ij} is less than 0.01, the spreading process is stopped. The pseudo-code for this algorithm is described in the Appendix.

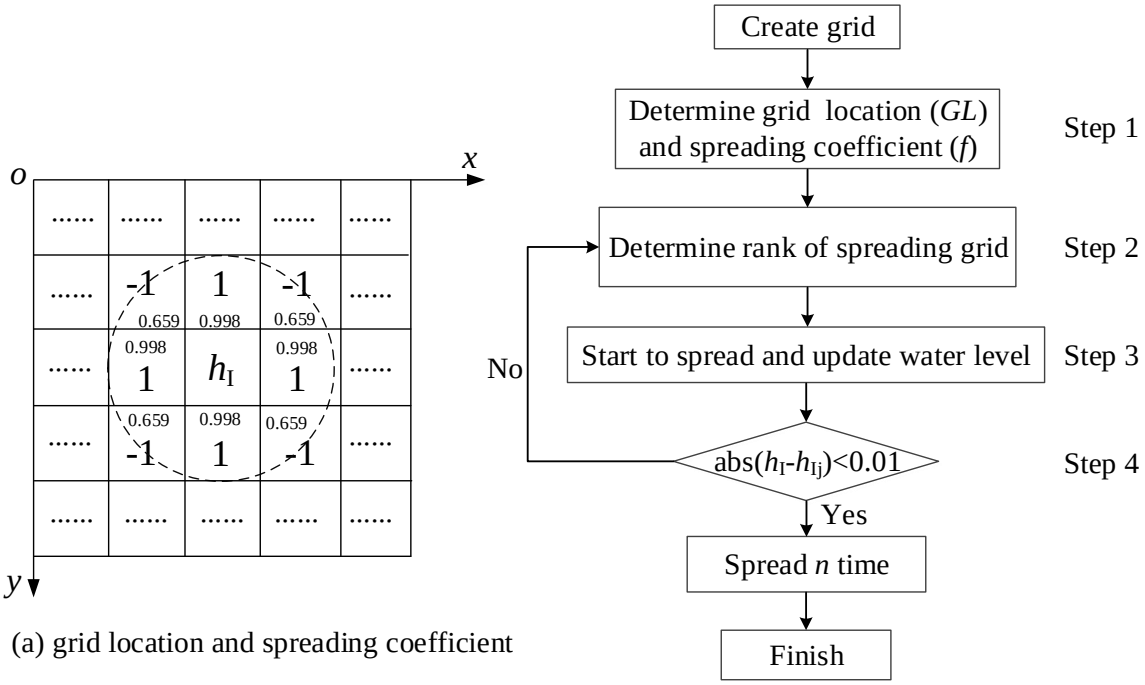

(a) grid location and spreading coefficient

(b) spreading procedure

Figure 3: Description of the spreading process: (a) determination of the grid location and spreading coefficient and (b) iterative calculation of the spreading process

The inundation depth around a metro station is used to evaluate the inundation risk of metro lines. Eq. (6) is proposed to qualitatively calculate the inundation depth around a metro station.

$$h_{t(station)} = (h_i - p) \times t - h_{0(station)} \tag{6}$$

where, $h_{t(\text{station})}$ is the inundation depth around the metro station, h_i is the inundation depth over the ground surface, p is the drainage capacity of the metro station, and $h_{0(\text{station})}$ is the step height of the metro station, (based on the standard of the design of a metro system, $h_{0(\text{station})} = 0.2$ m). When $h_{t(\text{station})} > 0$, the metro station will become inundated.

3.3 Model calibration and visualization

During the establishment of the storm water model in the SWMM, the rainfall intensity is set as the return

period of 50-year, 100-year, and 500-year. The simulation time period is set as 2 h. The runoff quantities of each subcatchment can be computed in the SWMM. Based on the obtained runoff volume, the inundation depth can be computed using the proposed algorithm. The inundation depth is used to evaluate the flood risks of the study area. Using the inundation depth of the ground surface, the inundation depth around a metro station can be yielded using Eq. (6). The spatial distribution of the inundation depth can be visualized by the GIS.

4. Results and analysis

4.1 Runoff volume

Fig. 4 shows the runoff volume of each subcatchment at different rainfall intensities. It can be seen that the runoff increasing with the increased rainfall intensity. Fig. 4 also depicts the area of each subcatchment. Most of the subcatchments cover approximately 2 km^2. The area of each subcatchment is used to calculate the average inundation depth. Then the average inundation depth is used to simulate the spreading process by employing the proposed algorithm. The computed results are incorporated GIS into SWMM to yield the map of the inundation distribution. Because the average inundation depth is related to the runoff volume and area of the subcatchment, the simulated results are able to reflect the surface runoff and overland flow of the study area. The algorithm plays an important role in analysing the spreading processes of the surface runoff volumes.

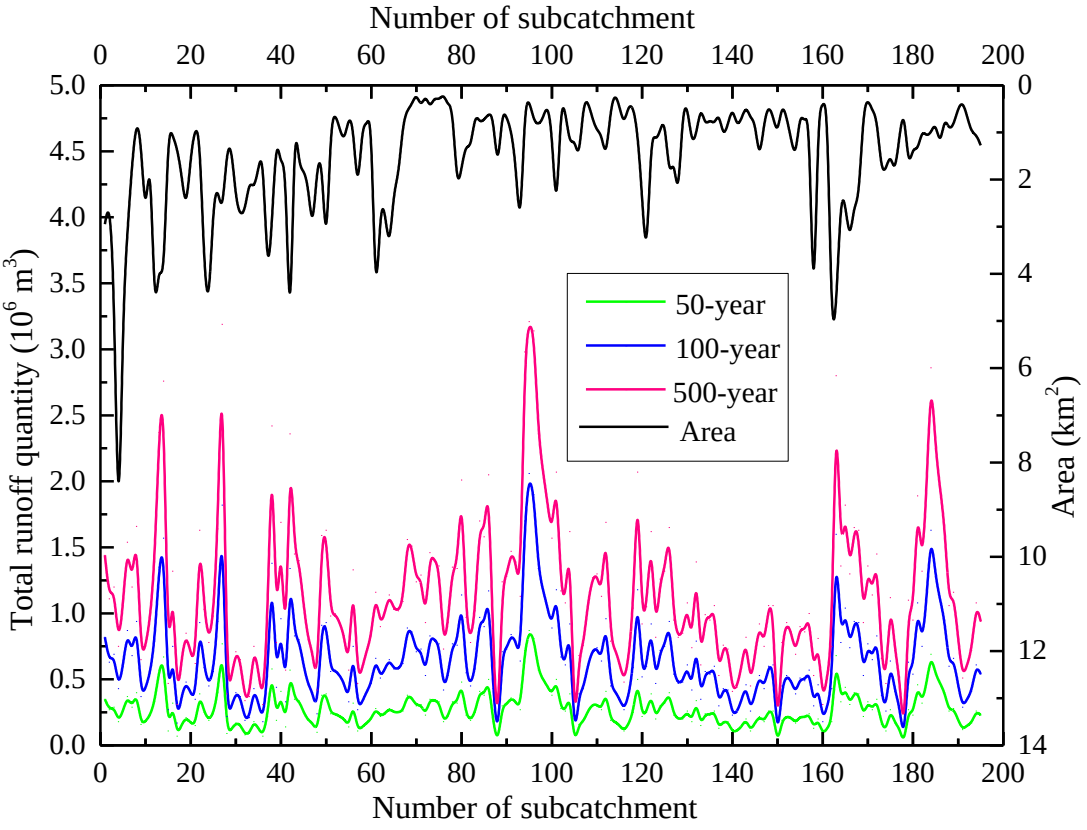

Figure 4: Runoff volume of each subcatchment in the corresponding area under different scenarios

4.2 Inundation extent and depth

The inundation depth across the study area can be computed using the proposed algorithm (see Fig. 3). Fig. 5 displays the distribution of the inundation extent and depth under the aforementioned rainfall scenarios. For all the three scenarios, the floodwater profiles are similar; however, the inundation depth and areal extent exacerbate with increasing rainfall intensity. Figs. 5a and 5b exhibit the similarities in both the inundation depth and extent for the different scenarios. Fig. 5c depicts the maximum inundation depth and extent for the 500-year-rainfall intensity. The largest depth in each scenario first occurs in some places in the Changning, Huangpu, and Yangpu districts. The maximum inundation depth exceeds 400 mm.

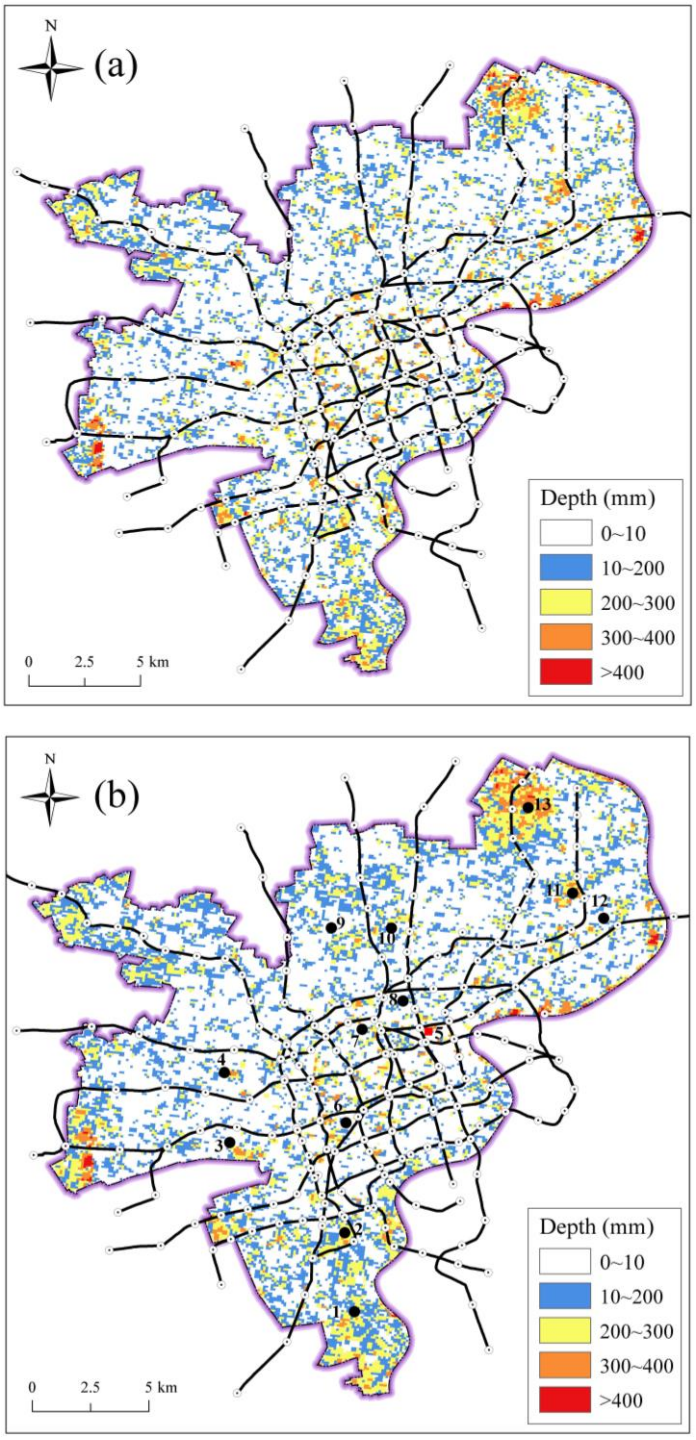

Figure 5: Distribution of the potential inundation extent and depth under different rainfall scenarios: (a) 50-year, (b) 100-year, and (c) 500-year-rainfall intensity (continuing)

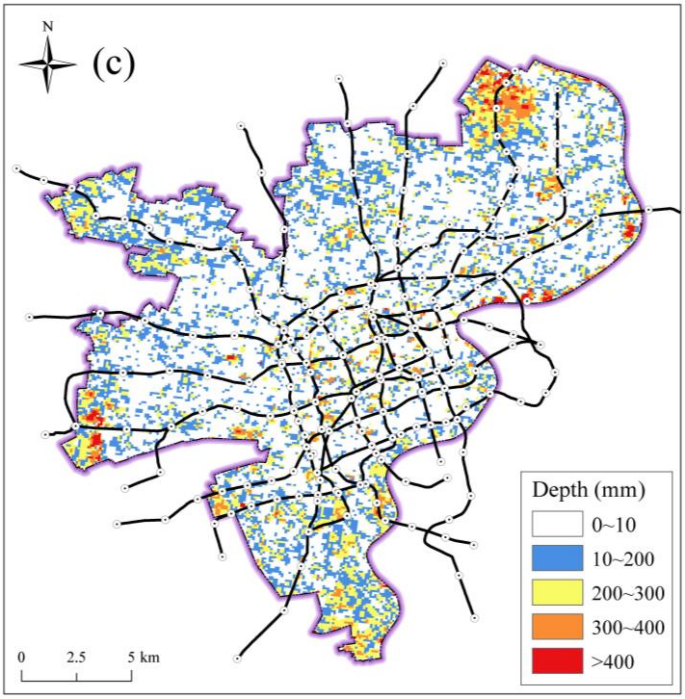

Figure 5: Distribution of the potential inundation extent and depth under different rainfall scenarios: (a) 50-year, (b) 100-year, and (c) 500-year-rainfall intensity (continued)

To analyse the inundation risk under different scenarios, the inundation area and inundated area ratios were accounted using the GIS. Fig. 6 presents the inundated area and ratio at different inundation depth ranges. As shown in Fig. 6, the inundated depth of 300 mm is a key point in the variation patterns under the three scenarios; specifically, when the inundated depth is over 300 mm, the inundated area increases with the increase in the rainfall scale, and when the inundated depth is less than 300 mm, the variation in the inundated area does not exhibit this pattern. To illustrate the variation in the inundated area and ratio for an inundation depth of over 300 mm, the detailed values of the inundation area and ratio in the depth range of 300–400 mm and over 400 mm are exhibited in Fig. 6. For the cases of inundation less than 300 mm, an irregular distributed pattern is formed for the inundated area, which may be due to the landform. The inundation area for an inundation depth of over 300 mm is up to 5.16 km^2 for the 500-year-rainfall intensity, which is 4.3% of the total studied area (120 km^2).

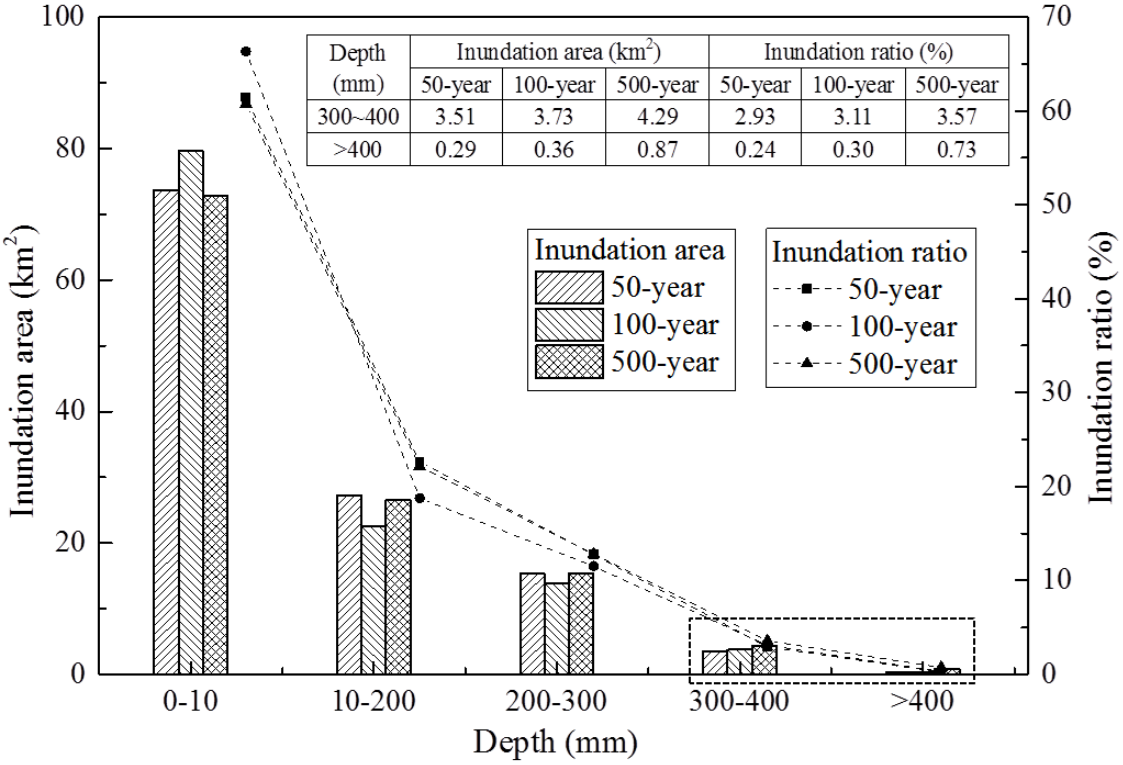

Figure 6: Statistical inundation area with the corresponding ratio at different depths

4.3 Potential inundation depth around metro station

Following the spatial distribution of the inundation depth of a ground surface, the potential inundation depth around metro stations can be obtained by applying Eq. (6). Fig. 7 shows the potential inundation depth around the metro stations under the scenarios of 50-year-rainfall intensity (Fig. 7a), 100-year-rainfall intensity (Fig. 7b), and 500-year-rainfall intensity (Fig. 7c). The inundated metro stations major occurred in the region with a deeper flood depth. As shown in Fig. 7, the inundation depths and extents exacerbate with increasing rainfall intensity. For the 50-year-rainfall intensity, the Xinjiangwan Cheng station, Yingao east station, Yangshupu Road station, and Longyao Road station are predicted to be inundated at 100 mm-depth. For the 100-year-rainfall intensity, the inundation depth of the four stations increased by 200–300 mm, whereas the inundation extent exacerbated to other central regions. For the

500-year-rainfall intensity, the largest inundation depth exceeds 300 mm, and other metro stations also undergo inundation with a depth of 100–300 mm in the central region. For all the three scenarios, the inundation initially occurs in the metro stations of Xinjiangwan Cheng, Yingao east, Yangshupu Road, and Longyao Road, and the depths increasing with the increased rainfall intensity.

The number of inundated stations can also be accounted from Fig. 7. It is clearly seen that with the increase in the rainfall intensity, the number of inundated metro stations is increasing. For the 500-year-rainfall intensity, the inundation depth of these stations of Xinjiangwan Cheng, Yingao east, Yangshupu Road, and Longyao Road over 300 mm (see Fig. 7c).

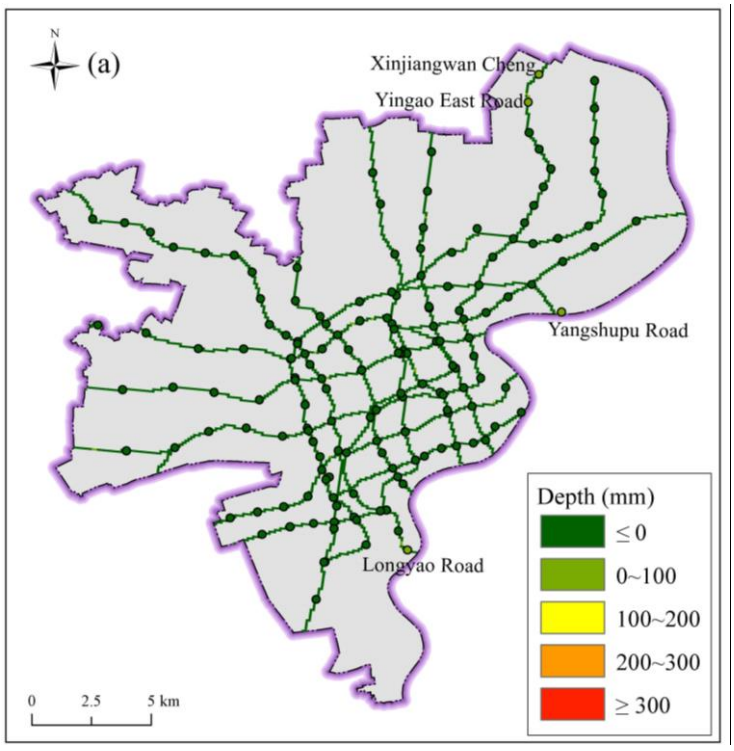

Figure 7: Potential inundation depth around the metro stations under different scenarios: (a) 50-year, (b) 100-year, and (c) 500-year-rainfall intensity (continuing)

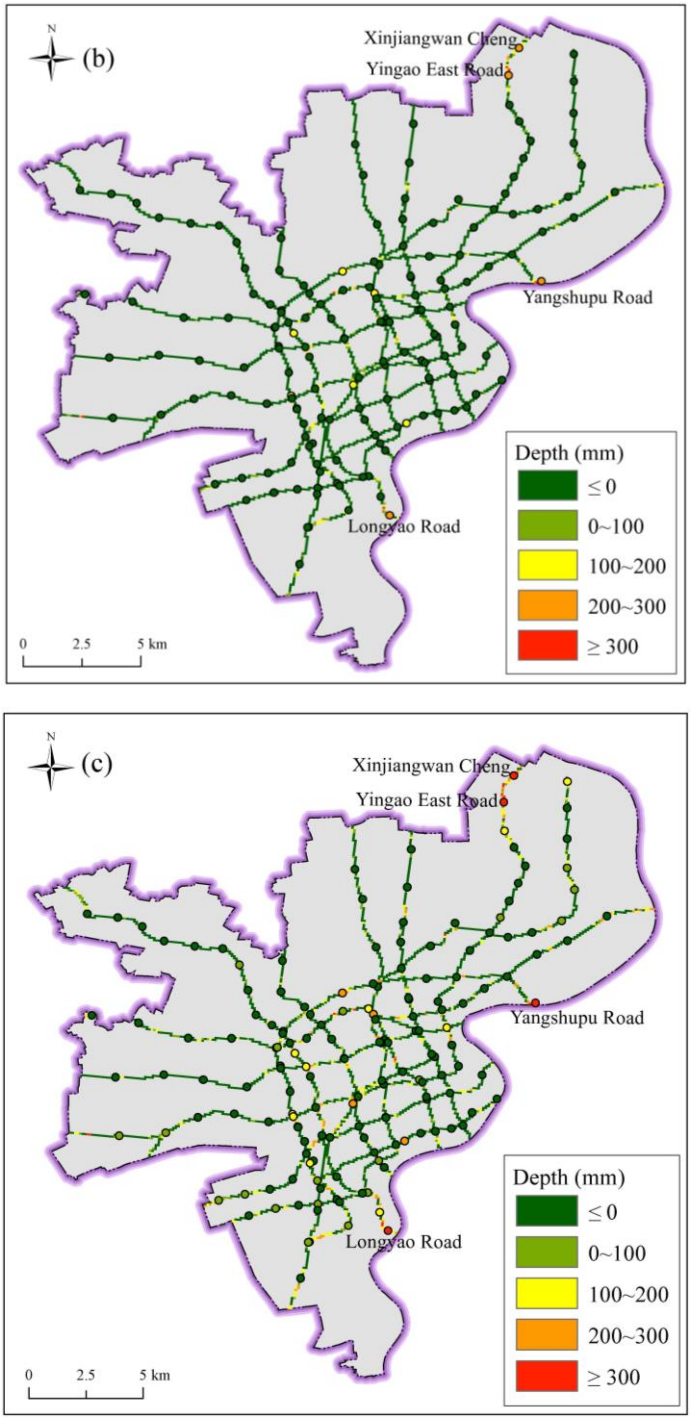

Figure 7: Potential inundation depth around the metro stations under different scenarios: (a) 50-year, (b) 100-year, and (c) 500-year-rainfall intensity (continued)

4.4 Model validation

For an effective validation of the proposed model, observed inundation maps from RS, such as aerial or satellite, and reliable field surveys must be compared with the calculated inundated areas. However, the observed inundation maps for historical flood events are not available for Shanghai. There are some historical recorded data of the inundated depth of several locations in Shanghai from public sources. Thus, the proposed model is validated by the comparison between the simulated data and these records of the historical floods. These records were collected from the following two sources: 1) flood incidents reported by public sources via websites (e.g., Google and Baidu), 2) publications (Huang et al. 2017; Yin et al. 2016b). The public sourced data provided enough information, which includes the location of the affected roads and buildings, with an estimate of the inundation depth. Fig. 8 depicts the location of the recorded flood. As presented in Fig. 8a, the records of the historical floods are located in the range with a deep inundation depth. Fig.8b shows the scene of the flooding of the Xujingdong road, which can be found online (http://www.miss-no1.com/file/2015/08/25/618466%40152054_1.htm). Fig. 8c shows the scene of the flooding of Yangshupu road, which can be accessed online (http://www.chexun.com/2013-10-09/102090984_2.html). The locations of these two flood incidents correspond with the simulated flood map (see Fig. 8a).

The other method for collecting the recorded flood data is the use of publications. The official records of the rainstorm which occurred with typhoon 'Matsa' in 2005 presented by Huang et al. (2017) are similar to the simulated 100-year-scenario, which caused serious inundation in the districts of Yangpu, Hongkou, Changning, Putuo, and Xuhui. In addition, Yin et al. (2016b) recorded the flood event which occurred on 12 August 2011, but this research analysed only an area of 3.25 km^2. Thus, only one validation point was extracted from Yin et al. (2016b). Finally, we collected 13 flooding locations as shown in Fig. 8a. In Fig. 8a, except for point 5, the points of the flood location were collected from the report of Huang et al.

(2017). Point 5 is collected from the paper of Yin et al. (2016b). From the collection of these recorded data, the simulated results were compared with the records at 13 validation points. Fig. 9 shows the comparison of the inundation depth obtained from the simulated results and recorded data. For point 2 to point 12, the simulated data agrees well with the recorded data with a relative difference of less than 10%, whereas the simulated data at points 1 and 13 are much deeper than the records. One possible reason for the difference between the simulated data and recorded data for points 1 and 13 could be the fixed boundary effect because these two points are near the boundary. In addition, point 5 is the flood location in 2011, which is deeper than the simulated data. Overall, the calculated results can reflect the trends of the floodwater movement and depth.

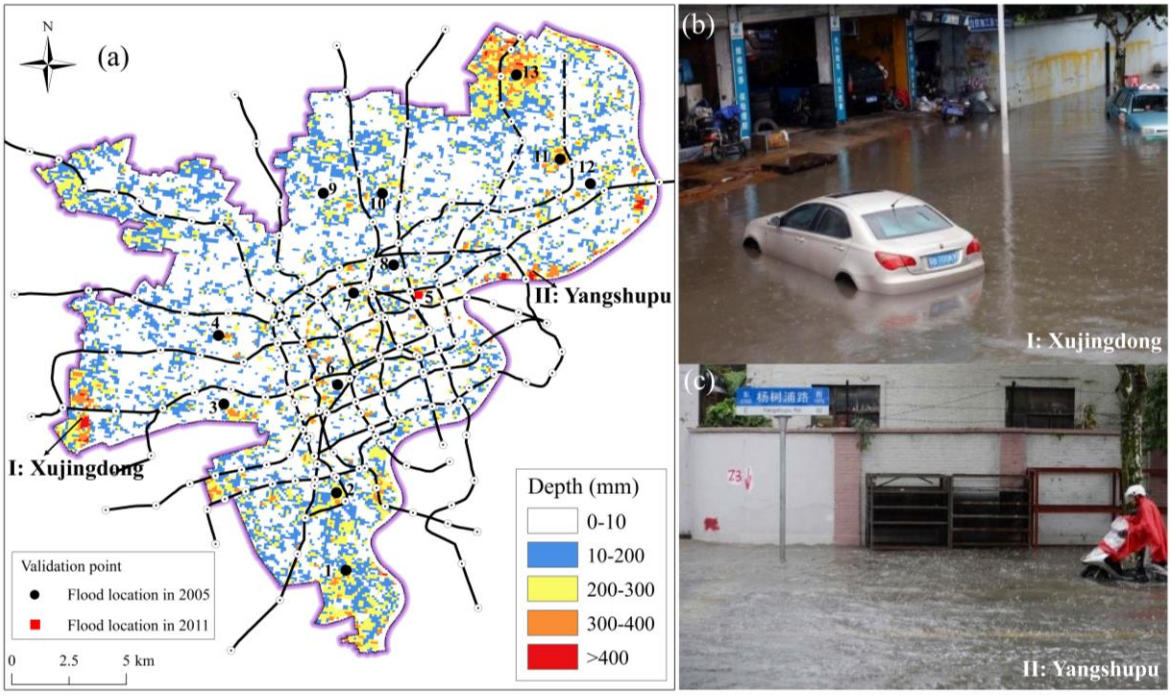

Figure 8: Distribution of the recorded flood locations: a) recorded flood locations, b) inundation of the Xujingdong road, and c) inundation of the Yangshupu road

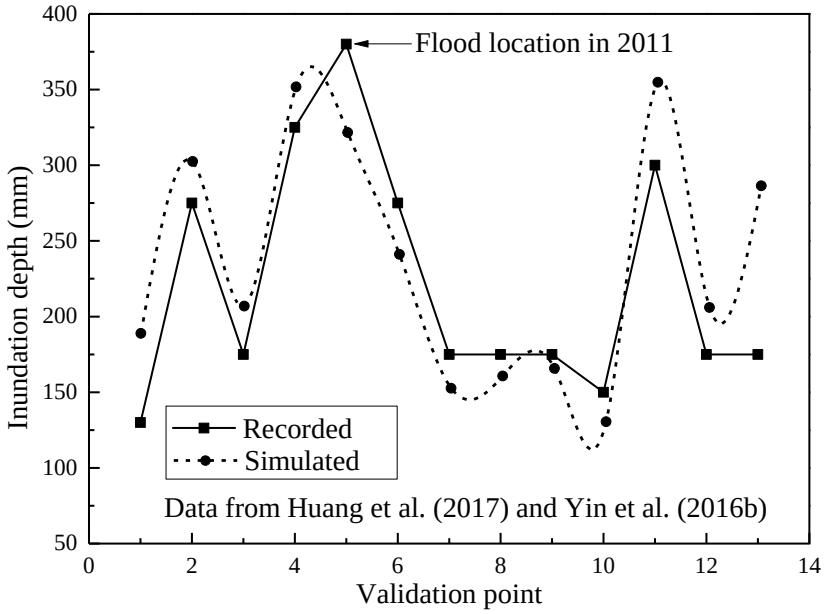

Figure 9: Comparison of the inundation depths obtained from the simulated results and recorded data

5. Discussion

5.1 Model evaluation and limitations

In this study, the open-source inundation model, SWMM, combines with the GIS is adopted to evaluate inundation risks. To improve the approach, a new algorithm is proposed to simulate the overland flow on the ground surface. The algorithm can integrate the SWMM into the GIS. The integrated approach can predict the inundation risks on a regional scale, whereas the existing methods can only evaluate a small area. It is supposed that the rainwater is flowed from one subcatchment to another. Moreover, a spreading coefficient is used for moving runoff between neighbouring subcatchments. During surface flowing, the rainwater is redistributed between ground surface and drainage station. The limitation of the integrated approach is that the existing drainage network has not directly considered during simulation, since the complexity of the drainage network in a regional scale. Alternatively, the capacity of the drainage station (see Fig. 2) is used to reduce the water quantity of each subcatchment calculated in SWMM. The function

of drainage network is reflected by the drainage capacity of each drainage station. The proposed algorithm is used to spreading surface flow based on the variation of the elevation in study area. Thus, the proposed approach is suitable to simulate the inundation risk in flat region. Because of a lack of recorded data for the inundation depths of metro stations, only the inundation depth on the ground surface is validated by the comparison between the simulated results and the records of historical floods. The comparison reveals that the model can capture the surface flowing dynamics of rainwater. However, there are also some differences between the calculated inundation depth and validated results. This may be ascribed to the uncertainties from various assumptions of the parametric values, data quality, and modelling conditions. These uncertainties result in a larger inundation depth than the recorded data. Overall, the simulated result can provide a relatively safe prediction of inundation risks. Although there are various uncertainties in the simulated results, the deviation is acceptable and model is satisfactory for urban inundation predictions.

5.2 Flooding prevention measures

The simulated results show a spatiotemporal distribution of the inundation profiles. The inundation profiles are characterized by a consistency in the rainfall scenarios with larger inundation depths and extents corresponding to higher rainfall intensities. In the scenario of the 500-year-rainfall intensity, various regions within the study area are predicted to suffer catastrophic inundation, particularly those regions near the Huangpu River. This phenomenon may be due to the backwater effect, which is well known to be stronger and more apparent at riversides than that in inland regions. Therefore, there is a need to improve the drainage facilities (e.g., sewer system, manhole, and outlet) along the Huangpu River. Inundation of the metro system primarily occurred in the regions with a deep inundation depth. To mitigate the damage caused by inundation in metro system, the drainage capacity of the ground surface around the metro station should be increased (Suarez et al. 2005; Aoki et al. 2016). In addition, the height of the step of the metro station with a high inundation risk should be increased. Drainage facilities within the metro station should also be allocated for the emergency of flooding. In the future, more flooding

adaptation measures should be taken to mitigate the catastrophic damages caused by urban flooding.

6. Conclusions

This paper presented a method to evaluate potential inundation risks through the integration of a hydraulic model and GIS-based analysis via a proposed algorithm. The proposed approach was used to predict the inundation risk of metro system of Shanghai. The results were verified by recorded flooding events. According to the results, major conclusions were drawn as follows:

(1) A new algorithm to simulate the overland flow was proposed to simulate the inundation extent and depth on the ground surface. This algorithm included two aspects: i) determination of the grid location and ii) an interactive calculation of the spreading process. With the proposed algorithm, the incorporated SWMM and GIS are adopted to yield a spatial-temporal distribution of the inundation risk on the ground surface.

(2) Based on the inundation depth on the ground surface, an equation to qualitatively calculate the inundation depth of the metro system was proposed. The proposed equation provided a quantitative evaluation of the metro system by considering the drainage capacity and characteristics of each metro station.

(3) The proposed approach was used to simulate the inundation risk of the metro stations in Shanghai under 50-year, 100-year, and 500-year scenarios. The results showed that these stations of Xinjiangwan Cheng, Yingao east, Yangshupu Road, and Longyao Road are possible to inundated. In the 50-year-rainfall intensity, these four stations are predicted to be inundated at 100 mm-depth. In the 100-year-rainfall intensity, the inundation depth of the four stations increased by 200–300 mm, whereas the inundation extent exacerbated to other central regions. In the 500-year-rainfall intensity, the largest inundation depth exceeds 300 mm, and other metro stations also undergo inundation with a depth of 100–300 mm in the central region.

(4) The drainage facilities should be improved to decrease the damage induced by urban floods, especially

for the regions with metro stations and high inundation risks. In addition, the height of the step for the metro stations with a high risk should be investigated in detail.

Acknowledgements. The research work described herein was funded by the National Natural Science Foundation of China (NSFC) (Grant No. 41672259). This financial support is gratefully acknowledged.

Author contribution. This paper represents a result of collaborative teamwork. Shui-Long Shen developed the concept; Hai-Min Lyu drafted the manuscript; Jun Yang provided constructive suggestions and revised the manuscript; Zhen-Yu Yin collected the data and revised the manuscript. The four authors contributed equally to this work.

Competing interests. The authors declare that they have no conflict of interest.

Appendix: Pseudo-code of the algorithm for the spreading procedure

Algorithm: Algorithm for the spreading process of the runoff volume.

input: Arcgis.in € (A, E, h, x, y)

! *Data with area, elevation, average water depth, and X/Y coordinates from the arcgis database.*

output: Data.out € (A, h`)

! *Water depth of each grid.*

Determine the relative location and spreading coefficient of each grid around the target grid.

Spreading process

Do i = 1, N

! *N is the iteration step of the spreading steps.*

Rank of spreading for each grid

$$Q_{target} = \sum_{i=1}^{link} h_i A_i$$

! *Based on the water quantity of each grid, select the target grid.*

Start spreading

Do n = 1, M

! *M is the total number of spreading grids. The maximum value of M=8.*

If ((**abs**(h_I-h_{Ij})>0.01) .and. Q_I>0) **Then**

$$Q_{diffuse} = \sum_{j=1}^{n} (h_I - h_{Ij}) \cdot A_j \quad (j=1,2,\cdots,n)$$

! *Based on the spreading coefficient, allocate the water quantity and update the water level of each grid around the target.*

End if

End do

End do

References

Aoki, Y., Yoshizawa, A., and Taminato, T.: Anti-inundation measures for underground stations of Tokyo Metro. Procedia Engineering. 165, 2-10, doi: 10.1016/j.proeng.2016.11.730, 2016.

Bisht, D.S, Chatterjee, C., Kalakoti, S., Upadhyay, P., Sahoo, M., Panda, A.: Modeling urban floods and drainage using SWMM and MIKE URBAN: a case study. Natural Hazards. 84: 749-776, **2016**.

Chang, H., Lafrenz, M., Jung, I.W., Figliozzi, M., Platman, D., and Pederson, C.: Potential impacts of climate change on flood-induced travel disruptions: a case study of Portland, Oregon, USA. Annals of the Association of American Geographers, 100(4), 938-952, doi: 10.1080/00045608.2010.497110, **2010**.

Chen, C.N., Tsai, C.H., Wu, M.H., and Tsai, C.T.: Numerical simulation of potential inundation in a coastal zone. Journal of Flood Risk Management, 8(3), 208-223, doi: 10.1111/jfr3.12088, **2015**.

Cherqui, F., Belmeziti, A., Granger, D., Sourdril, A., and Le Gauffre, P.: Assessing urban potential flooding risk and identifying effective risk-reduction measures. Science of the Total Environmental. 514, 418–425, doi: 10.1016/j.scitotenv.2015.02.027, **2015**.

DGJ08-37-2012. Code for investigation of geotechnical engineering in Shanghai. Shanghai Urban Construction and Communications Commission, Shanghai. (in Chinese), **2012**.

Feng, Y., Burian, S., and Pomeroy, C.: Potential of green infrastructure to restore predevelopment water budget of a semi-arid urban catchment. Journal of Hydrology, 542, 744-755, doi: 10.1016/j.jhydrol.2016.09.044, **2016.**

Han, K., Kim, Y., Kim, B., Famiglietti, J.S., and Sanders, B.F.: Calibration of stormwater management model using flood extent data. Proceedings of the ICE-Water Management, 167(1), **2014**.

Hashimoto, H., Park, K., and Watanabe, M.: Overland flood flow around the JR Hakata-eki station from the Mikasa and Sanno-Channel River in Fukuoka City on June 29, 1999. Journal of Japan Society for Natural Disaster Science. 21(4), 369-384, **2003**.

Herath, S. and Dutta, D.: Modeling of urban flooding including underground space. In Proceedings of the Second International Conference of Asia-Pacific Hydrology and Water Resources Association (pp. 55-63). **2004**.

Horritt, M.S., and Bates, P.D.: Evaluation of 1D and 2D numerical models for predicting river flood inundation. Journal of Hydrology. 268(1), 87-99, doi: 10.1016/S0022-1694(02)00121-X, **2002**.

Hsu, M.H., Chen, S.H., and Chang, T.J.: Inundation simulation for urban drainage basin with storm sewer system. Journal of Hydrology, 234(1-2), 21-37, doi: 10.1016/S0022-1694(00)00237-7, **2000**.

Huong, H.T.L. and Pathirana, A.: Urbanization and climate change impacts on future urban flooding in Can Tho city, Vietnam. Hydrology and Earth System Sciences. 17(1), 379-394, doi: 10.5194/hess-17-379-2013, **2013**.

Huang, Q., Wang, J., Li, M., Fei, M., and Dong, J.: Modeling the influence of urbanization on urban pluvial flooding: a scenario-based case study in Shanghai, China. Natural Hazards. 87(2), 1035-1055, doi: 10.1007/s11069-017-2808-4, **2017**.

Ishigaki, T., Kawanaka, R., Onishi, Y., Shimada, H., Toda, K., and Baba, Y.: Assessment of safety on evacuating route during underground flooding. In Advances in Water Resources and Hydraulic Engineering (pp. 141-146). Springer, Berlin, Heidelberg, **2009**.

Jiang, M.: Revision of Shanghai stromwater intensity formula under new stromwater situation. China Water and Wastewater. 31(15), 114-117, **2015**, (in Chinese).

Jiang, W., Deng, L., Chen, L., Wu, J., and Li, J.: Risk assessment and validation of flood disaster based on fuzzy mathematics. Progress in Natural Science. 19 (10), 1419–1425, doi: 10.1016/j.pnsc.2008.12.010, **2009**.

Kazakis, N., Kougias, I., and Patsialis, T.: Assessment of flood hazard areas at a regional scale using an index-based approach and analytical hierarchy process: application in Rhodope–Evros region, Greece. Science of Total Environment. 538, 555–563, doi: 10.1016/j.scitotenv.2015.08.055, **2015**.

Lee, S.B., Yoon, C.G., Jung, K.W., and Hwang, H.S.: Comparative evaluation of runoff and water quality using HSPF and SWMM. Water Science and Technology. 62 (6), 1401–1409, doi: 10.2166/wst.2010.302, **2010**.

Lyu, H.M., Wang, G.F., Shen, J.S., Lu, L.H., and Wang, G.Q.: Analysis and GIS mapping of flooding hazards on 10 May, 2016, Guangzhou, China. Water. 8, 447(1-17). doi: 10.3390/w8100447, **2016**.

Lyu, H.M., Wang, G.F., Cheng, W.C., and Shen, S.L.: Tornado hazards on June 23rd in Jiangsu Province, China: Preliminary investigation and analysis. Natural Hazards. 85, 597–604, doi: 10.1007/s11069-016-2588-2, **2017**.

Lyu, H.M., Sun, W.J., Shen, S.L., and Arulrajah, A.: Flood risk assessment in metro systems of mega-cities using a GIS-based modeling approach. Science of the Total Environment, 626, 1012-1025. doi: 10.1016/j.scitotenv.2018.01.138, **2018**a.

Lyu, H.M., Xu, Y.S., Cheng, W.C., and Arulrajah, A.: Flooding hazards across southern China and prospective sustainability measures. Sustainability, 10(5), 1682. doi:10.3390/su10051682, **2018**b.

Lyu, H.M., Shen, S.L., Zhou, A.N., and Yang, J.: Perspectives for flood risk assessment and management for mega-city metro system. Tunneling and Underground Space Technology, 84(2019), 31-44. https://doi.org/10.1016/j.tust.2018.10.019, **2019**.

Meesuk, V., Vojinovic, Z., Mynett, A.E., and Abdullah, A.F.: Urban flood modelling combining top-view LiDAR data with ground-view SfM observations. Advances in Water Resources. 75, 105–117, doi: 10.1016/j.advwatres.2014.11.008, **2015**.

Morales-Hernandez, M., Petaccia, G., Brufau, P., and García-Navarro, P.: Conservative 1D–2D coupled numerical strategies applied to river flooding: The Tiber (Rome). Applied Mathematical Modelling, 40(3), 2087-2105, **2016**.

Naulin, J.P., Payrastre, O., and Gaume, E.: Spatially distributed flood forecasting in flash flood prone areas: Application to road network supervision in Southern France. Journal of Hydrology. 486, 88-99, doi: 10.1016/j.jhydrol.2013.01.044, **2013**.

Nott, J.: Extreme events: A physical reconstruction and risk assessment. Cambridge University Press., **2006.**

Peng, J. and Peng, F.L.: A GIS-Based evaluation method of underground space resource for urban spatial planning: Part 1 methodology. Tunnelling and Underground Space Technology. 74, 82-95, doi: 10.1016/j.tust.2018.01.002, **2018**.

Quan, R., Zhang, L., Liu, M., Lu, M., Wang, J., and Niu, H.: Risk assessment of rainstorm waterlogging on subway in central urban area of Shanghai, China based on scenario simulation. The 19th International Conference on Geoinformatics. pp: 1-6, **2011**.

Sampson, C.C., Fewtrell, T.J., Duncan, A., Shaad, K., Horritt, M.S., and Bates, P.D.: Use of terrestrial laser scanning data to drive decimetric resolution urban inundation models. Advances in Water Resources. 41, 1–17, doi:

10.1016/j.advwatres.2012.02.010, **2012**.

Shen, J. and Zhang, Q.W.: A GIS-based subcatchments division approach for SWMM. Open Civil Engineering Journal. 9, 515-521, doi: 10.2174/1874149501509010515, **2015**.

Shen, S.L., Wang, J.P., Wu, H.N., Xu, Y.S., Ye, G.L., and Yin, Z.Y. (2015). Evaluation of hydraulic conductivity for both marine and deltaic deposits based on piezocone testing. Ocean Engineering, 110(2015), 174-182. doi: 10.1016/j.oceaneng.2015.10.011, **2015**.

Shen, S.L. and Xu, Y.S.: Numerical evaluation of land subsidence induced by groundwater pumping in Shanghai. Canadian Geotechnical Journal. 48(9), 1378-1392, doi: 10.1139/t11-049, **2011**.

Shen, S.L., Wu, H.N., Cui, Y.J., and Yin, Z.Y.: Long-term settlement behavior of the metro tunnel in Shanghai, Tunneling and Underground Space Technology, 40(2014), 309-323, doi: 10.1016/j.tust.2013.10.013, **2014**.

Shen, S.L., Wu, Y.X., and Misra, A.: Calculation of head difference at two sides of a cut-off barrier during excavation dewatering. Computers and Geotechnics. 91, 192-202, doi: 10.1016/j.compgeo.2017.07.014, **2017**.

Suarez, P., Anderson, W., Mahal, V., and Lakshmanan, T.R.: Impacts of flooding and climate change on urban transportation: a systemwide performance assessment of the Boston Metro Area. Transportation Research Part D: Transport and Environment. 10(3), 231-244, doi: 10.1016/j.trd.2005.04.007, **2005**.

Szydlowski, M., Szpakowski, W., and Zima, P.: Numerical simulation of catastrophic flood: the case study of hypothetical failure of the Bielkowo hydro-power plant reservoir. Acta Geophysica, 61(5), 1229-1245, doi: 10.2478/s11600-013-0104-6, **2013**.

Tan, S.B., Chua, L.H., Shuy, E.B., Lo, E.Y.M., and Lim, L.W.: Performances of rainfall-runoff models calibrated over single and continuous storm flow events. Journal of Hydrologic Engineering. 13(7), 597–607, doi: 10.1061/(ASCE)1084-0699(2008)13:7(597), **2008**.

Tan, Y., Zhu, H., Peng, F., Karlsrud, K., and Wei, B.: Characterization of semi-top-down excavation for subway station in Shanghai soft ground. Tunneling Underground Space Technology. 68: 244–261, doi: 10.1016/j.tust.2017.05.028, **2017**.

Willems, P.: Revision of urban drainage design rules after assessment of climate change impacts on precipitation extremes at Uccle, Belgium. Journal of Hydrology. 496, 166–177, doi: 10.1016/j.jhydrol.2013.05.037, **2013**.

Wu, X.S., Wang, Z.L., Guo, S.L., Liao, W.L., Zeng, Z.Y., and Chen, X.H.: Scenario-based projections of future urban inundation within a coupled hydrodynamic model framework: A case study in Dongguan City, China. Journal of Hydrology. 547, 428-442, doi: 10.1016/j.jhydrol.2017.02.020, **2017**.

Wu, J.S., Yang, R., Song, J.: Effectiveness of low-impact development for urban inundation risk mitigation under different scenarios: a case study in Shenzhen, China. Natural Hazards and Earth System Science. 18: 2525-2018, **2018**.

Wu, Y.X., Shen, S.L., and Yuan, D.J.: Characteristics of dewatering induced drawdown curve under blocking effect of retaining wall in aquifer. Journal of Hydrology. 539: 554-566, doi: 10.1016/j.jhydrol.2016.05.065, **2016**.

Xia, J., Falconer, R.A., Lin, B., and Tan, G.: Numerical assessment of flood hazard risk to people and vehicles in flash floods. Environmental Modelling & Software. 26(8), 987-998, doi: 10.1016/j.envsoft.2011.02.017, **2011**.

Xu, Y.S., Shen, S.L., Lai, Y., and Zhou, A.N.: Design of Sponge City: lessons learnt from an ancient drainage system in

Ganzhou, China. Journal of Hydrology, 563(2018), 900-908, doi: 10.1016/j.jhydrol.2018.06.075, **2018**.

Yanai, T.: The actual situations and measures of floods in underground spaces, Fukuoka City. Rainwater Technical Report. 37, 19-23, **2000**.

Yin, J., Yu, D.P., Yin, Z.E., Liu, M., and He, Q.: Evaluating the impact and risk of pluvial flash flood on intra-urban road network: A case study in the city center of Shanghai, China. Journal of Hydrology. 537, 138-145, doi: 10.1016/j.jhydrol.2016.03.037, **2016**a.

Yin, J., Yu, D., and Wilby, R.: Modelling the impact of land subsidence on urban pluvial flooding: A case study of downtown Shanghai, China. Science of the Total Environment. 544, 744-753, doi: 10.1016/j.scitotenv.2015.11.159, **2016**b.

Yin, Z.Y., Jin, Y.F., Shen, J.S., and Hicher, P.Y.: Optimization techniques for identifying soil parameters in geotechnical engineering: comparative study and enhancement. International Journal for Numerical & Analytical Methods in Geomechanics, 42:70–94, doi: 10.1002/nag.2714, **2018**.

Zhao, G., Xu, Z.X., Pang, B., Tu, T.B., Xu, L.Y., Du, L.G.: An enhanced inundation method for urban flood hazard mapping at the large catchment scale. Journal of Hydrology. 571: 873-882, **2019**.

Zhou, Q., Mikkelsen, P.S., Halsnæs, K., and Arnbjerg-Nielsen, K.: Framework for economic pluvial flood risk assessment considering climate change effects and adaptation benefits. Journal of Hydrology. 414, 539-549, doi: 10.1016/j.jhydrol.2011.11.031, **2012**.

Zhu, Z., Chen, Z., Chen, X., and He, P.: Approach for evaluating inundation risks in urban drainage systems. Science of the Total Environment. 553, 1-12, doi: 10.1016/j.scitotenv.2016.02.025, **2016**.